



Alterations in the surface properties of sea spray aerosols introduced by the presence of sterols

Shumin Cheng, Siyang Li, Narcisse Tsona, C. George, Lin Du

► To cite this version:

Shumin Cheng, Siyang Li, Narcisse Tsona, C. George, Lin Du. Alterations in the surface properties of sea spray aerosols introduced by the presence of sterols. *Science of the Total Environment*, Elsevier, 2019, 671 (—), pp.1161-1169. 10.1016/j.scitotenv.2019.03.433 . hal-02166661

HAL Id: hal-02166661

<https://hal.archives-ouvertes.fr/hal-02166661>

Submitted on 1 Dec 2019

HAL is a multi-disciplinary open access archive for the deposit and dissemination of scientific research documents, whether they are published or not. The documents may come from teaching and research institutions in France or abroad, or from public or private research centers.

L'archive ouverte pluridisciplinaire **HAL**, est destinée au dépôt et à la diffusion de documents scientifiques de niveau recherche, publiés ou non, émanant des établissements d'enseignement et de recherche français ou étrangers, des laboratoires publics ou privés.

Alterations in the surface properties of sea spray aerosols introduced by the presence of sterols

Shumin Cheng,^a Siyang Li,^a Narcisse T. Tsona,^b Christian George,^{c,d} and Lin Du^{a,*}

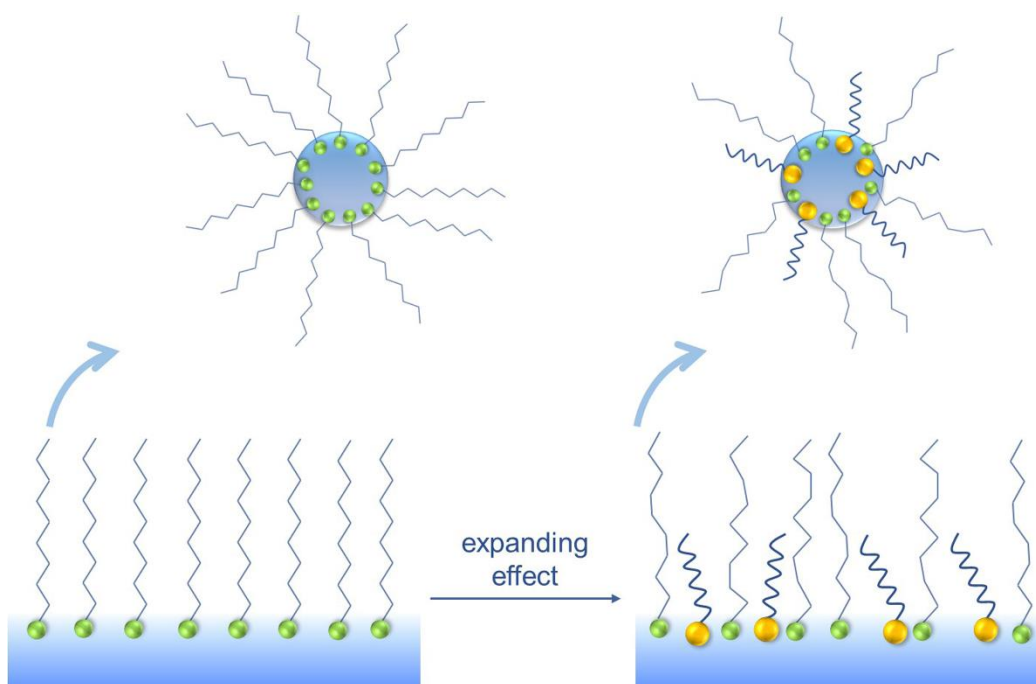
^a Environment Research Institute, Shandong University, Binhai Road 72, Qingdao 266237, China

^b School of Life Science, Shandong University, Binhai Road 72, Qingdao 266237, China

^c School of Environmental Science and Engineering, Shandong University, Binhai Road 72, Qingdao 266237, China

^d University of Lyon, Université Claude Bernard Lyon 1, CNRS, IRCELYON, F-69626 Villeurbanne, France

Corresponding author: Email: lindu@sdu.edu.cn, Tel: +86-532-58631980



17 **Abstract**

18 The mixed steric acid (SA)/sterol systems were used as sea spray aerosol mimics to get more insights
19 into the alterations in surface properties of aerosols induced by sterols. By means of surface pressure
20 (π)-area (A) isotherms and polarization modulation-infrared reflection absorption spectroscopy (PM-
21 IRRAS), the effect of cholesterol (chol), stigmasterol (stig) and ergosterol (erg) on the lateral packing
22 and chain conformation of SA monolayer was explored. The fact that the excess areas of mixing of
23 the mixed monolayers exhibit significant deviations from ideally mixed film proves that, the sterols
24 are miscible with SA in the whole range of the monolayer compositions and surface pressures. The
25 lift-off areas in π -A isotherms were found to increase with increasing mole fraction of sterols,
26 indicating that expulsive interactions exist between SA and sterols, which are more pronounced when
27 the mole fraction of sterols is 0.7. In addition, the peak intensities of $\nu_a(\text{CH}_2)$ and $\nu_s(\text{CH}_2)$ in IRRAS
28 spectra decrease with increasing sterols levels, which is consistent with our findings in the π -A
29 isotherms, that the addition of sterols leads to a looser chain packing in SA monolayer. The proportion
30 of *gauche* defects in SA monolayer induced by the sterols follows the order cholesterol < stigmasterol
31 < ergosterol at a certain sterol level, as reflected by the decreasing peak intensities of $\nu_a(\text{CH}_2)$ and
32 $\nu_s(\text{CH}_2)$. Consequently, the sterols generally give rise to considerable expanding effects on SA
33 monolayer, which are particularly pronounced for stigmasterol and ergosterol, suggesting that the
34 additional alkyl side chains and double bonds of the sterols play a role on disordering SA monolayer.
35 The present study is likely to shed light on many boundary processes take place at the interface of
36 SSAs, in particular, transport processes of water and trace gases across the interface.

37 **Keywords:** Langmuir films; Fatty acid; Sterol; Expanding effect; Mixed monolayer

38 **Highlights:**

39 High orderly packed SA monolayer undergoes expansion upon addition of sterols;

40 The phase behavior of SA/sterol mixed monolayers are dominated by sterols;

41 The bulkier hydrophobic portion of stigmasterol and ergosterol result in reduced packing
42 effectiveness;

43 A looser chain packing facilitate transport of water and reactive trace gases across the interface.

44 **1. Introduction**

45 The sea surface microlayer (SML) is generally enriched in organic substances, particularly
46 amphiphile ones, which accumulate at the air-sea interface due to their surface-active properties. Sea
47 spray aerosols (SSAs) mainly formed at during the bubble bursting (Adams et al., 2016; Prather et
48 al., 2013; Tseng et al., 1992) convey surface-active organics, selectively transferred to the aerosol
49 phase depending on their solubility and surface activity (Cochran et al., 2016a). The partitioning of
50 the organics to the air-water interface of SSAs leads to the formation of an organic coating, which
51 has been proposed to exist as inverted micelle structure with the hydrophilic head-group oriented into
52 the water droplet and the hydrophobic chain oriented outward (Ellison et al., 1999). Interfacial
53 characteristics of adsorbed organic coating films on SSAs alter their physical (Garland et al., 2005;
54 Noziere et al., 2014), chemical (Gilman et al., 2006; Rouviere and Ammann, 2010; Tinel et al., 2016)
55 and optical properties (Adams et al., 2016; Vaida, 2016), depending on the nature (i.e., characteristics
56 of the polar groups and structure of the hydrophobic chain) of the constituent organic compounds,
57 which in turn have effects on many atmospheric processes (Garland et al., 2005; McNeill et al., 2006).

58 Langmuir trough has been traditionally used for surface pressure (π)–area (A) isotherms to reveal
59 macroscopic phase behavior of surface films (Tang et al., 2010). The π –A isotherms obtained using
60 Langmuir trough can reveal fundamental information about the packing of molecules over a range of
61 molecular areas, and are also helpful for determining miscibility of components in binary systems
62 (Serfis et al., 2001). In addition, Langmuir monolayer techniques have been combined with various
63 spectroscopic and microscopic measurements such as polarization modulation-infrared reflection
64 absorption spectroscopy (PM-IRRAS) (Goto and Caseli, 2013), attenuated total reflection-infrared
65 spectroscopy (ATR-IR) (Mao et al., 2013), Brewster angle microscopy (BAM) (Tang et al., 2010),
66 fluorescence microscopy (FM) and atomic force microscopy (AFM) (Goto and Caseli, 2013) to
67 evaluate the morphological and molecular properties of monolayers. Among these techniques, PM-
68 IRRAS has emerged as one of the leading methods for detailed analyses of monolayers at the air-
69 water interface and can provide abundant information concerning lipid conformation, tilt, and head-
70 group structures (Du and Wang, 2007). This technique is currently an important in-situ method
71 coupled to Langmuir trough to directly monitor the interfacial properties of natural aqueous aerosols
72 under a simplified and controlled physicochemical environment (Shrestha et al., 2018).

73 The presence of significant portions of fatty acids with saturated and unsaturated alkyl chains at
74 the sea surface microlayer has been widely studied (Shrestha et al., 2018). Being single chain
75 amphiphilic molecules with high surface activity, fatty acids can be transferred to marine aerosols

76 during the bubble bursting process with higher efficiency relative to other less surface-active
77 molecules (Cochran et al., 2016a). Phospholipids from the marine biota are reported to be an
78 important source of saturated fatty acids found in the SML, and at the interface of marine aerosols
79 (Ellison et al., 1999; Zhang et al., 2016). Saturated fatty acids especially palmitic acid and stearic acid
80 (SA) are known to be the major SSA film forming materials, and thus thoroughly studied as Langmuir
81 monolayer in pure form or mixtures to elucidate their functions at interfaces of SSAs (Adams and
82 Allen, 2013; Adams et al., 2016; Griffith et al., 2013; Shrestha et al., 2018).

83 Previous detailed analysis of chemical compositions of samples from the air-sea interface has
84 found very high relative abundance of sterols, which indicate a substantial marine origin (Gasparovic
85 et al., 2008). Marine aerosols and SML water samples were collected for sterol analyses by gas
86 chromatography-mass spectrometry (Barbier et al., 1981). Sterols of various structures were detected
87 from both aerosol and seawater samples, with a large predominance of cholesterol over other sterols
88 (Barbier et al., 1981; Saliot and Barbier, 1973). Sterols are abundant and essential lipid component
89 of cell membranes of marine animals and plants (Gašparović et al., 1998; Su et al., 2007). There are
90 various sterols with different molecular structures such as cholesterol, stigmasterol and ergosterol
91 (Fig. S1). The latter two sterols differ from cholesterol in the structure of the side chain and the steroid
92 ring. Both stigmasterol and ergosterol contain an additional *trans* double bond between C22 and C23.
93 Ergosterol possesses a methyl group while stigmasterol possesses an ethyl group at C24. Moreover,
94 the ergosterol molecule has an additional double bond between C7 and C8, while the other two sterols
95 do not have. The influence of the addition of sterols on the properties of various lipid monolayers has
96 been well studied (Gagos and Arczewska, 2012; Minones et al., 2009). Cholesterol as well as other
97 sterols is known to influence the conformational order of the lipid alkyl carbon chains (Khattari et al.,
98 2017; Motomura et al., 1976). A former investigation by the Langmuir monolayer film technique
99 found that sitosterol and stigmasterol interact less effectively than cholesterol with the phospholipid
100 (Su et al., 2007). It can thus be speculated that the molecular structures of sterols also play an
101 important role in their interactions with the long chain fatty acids.

102 Mixed Langmuir monolayers are monomolecular films containing more than one film-forming
103 chemical component. Considering the chemical complexity of SML from which the SSAs stem,
104 mixed films are more representative proxies of organic coatings than homogeneous monolayers
105 because the intermolecular forces between the various film components in a mixed film may alter its
106 properties. In this work, binary systems consisting of SA and sterols of different molecular structures

107 (cholesterol, stigmasterol and ergosterol) were used as proxies of organic coating films of SSAs. The
108 use of sterols as one of the binary components in the mixed systems allows us to interpret the changes
109 in interfacial properties induced by lipids with structures significantly different from that of SA. The
110 Langmuir trough was used in combination with the IRRAS technique to study the surface behavior,
111 molecular packing and interactions in mixed SA/sterol systems. Based on the experimental
112 explorations, this work aims to clarify the underlying mechanisms of molecular interactions inside
113 the SA/sterol monolayers, and provide insights into the alterations in surface properties of SSAs
114 induced by the presence of sterols.

115 **2. Experimental section**

116 **2.1. Materials**

117 Stearic acid “SA” (98%, Aladdin), cholesterol “chol” (95%, Acros), ergosterol “erg” (96%, Alfa) and
118 “stig” stigmasterol (95%, Ark) were used as received. Monolayers were prepared on ultrapure water
119 subphase. The water was purified through a Millipore Milli-Q purification system that provides
120 ultrapure water of 18 M Ω cm resistivity. SA and sterols were dissolved in chloroform to obtain a
121 concentration of 1 mM, separately.

122 **2.2. Monolayer spreading and isotherm measurements**

123 A Langmuir trough was used to record the surface pressure–area isotherms of the monolayers at 294
124 \pm 1 K. The trough was made out of Teflon, and has an initial open area of 210 cm². The trough was
125 placed on an anti-vibration table and isolated from the environment using a Plexiglas cabinet. Two
126 motorized barriers sitting at two ends of the trough were used to compress the monolayer films while
127 a Wilhelmy plate hanging from a pressure sensor detected the change of surface pressure. The
128 Wilhelmy plate was made from a piece of rectangular filter paper, which can monitor the surface
129 pressure with a high accuracy of \pm 0.1 mN/m. The chloroform solutions of SA and sterols were used
130 to make up mixtures with molar ratios of $X_{\text{sterol}} = 0, 0.1, 0.3, 0.5, 0.7$ and 1. The trough was first filled
131 with pure water as the subphase. Tens of microliters of samples composed of either SA, sterol or
132 mixtures of them were then spread over the pure water subphase in a dropwise manner using a
133 micrometric syringe. Prior to beginning each compression, about 15 min was allowed for solvent
134 evaporation and monolayer relaxation. The compression of monolayer films was conducted at a
135 constant rate of 3 mm/min.

136 **2.3. PM-IRRAS measurements**

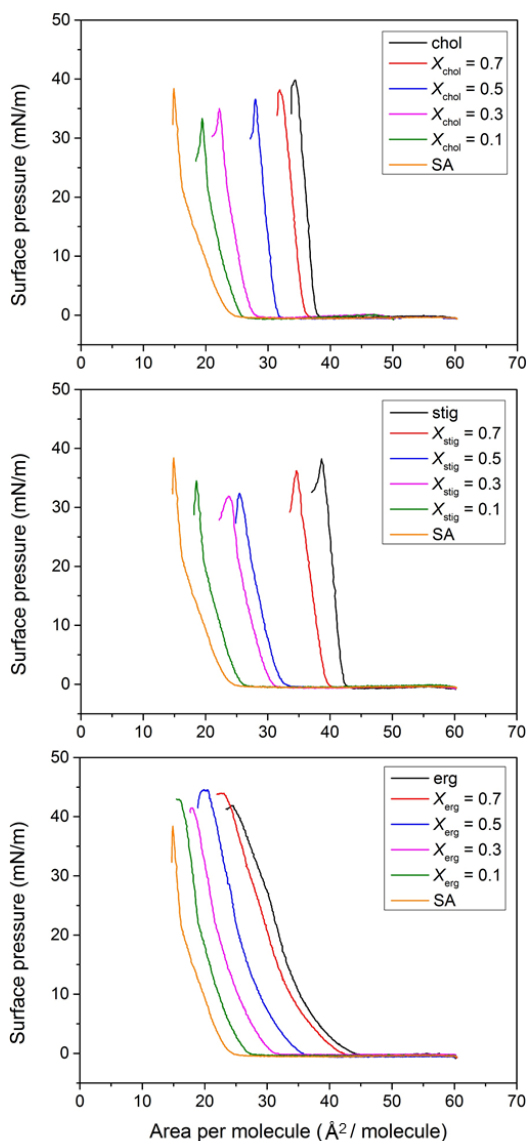
137 Polarization modulation-infrared reflection absorption spectroscopy (PM-IRRAS) measurements
138 were performed by combining a Bruker Vertex 70 FTIR spectrometer with an external variable angle
139 reflectance accessory (XA-511). The Langmuir trough described above was used to deposit films for
140 the PM-IRRAS studies. For IRRAS spectra collection, adsorbed films were compressed to the surface
141 pressure of 26 mN/m and maintained constantly with a deviation of ± 0.2 mN/m. A time delay of 60
142 s was allowed for film equilibrium between trough movement and data collection. To have maximum
143 signal strength, the angle of incidence of the IR light beam was set at 40° relative to the surface
144 normal. A ZnSe polarizer was used to generate perpendicularly polarized lights. The incoming light
145 was polarized by the polarizer and continuously modulated between s- and p-polarization at a high
146 frequency of 42 kHz by a photoelastic modulator, so that the spectra for the two polarizations can be
147 measured simultaneously. The difference between the s and p spectra provides information on the
148 species present at the interface, while the sum is the reference spectrum (Goto and Caseli, 2013). In
149 this way, the effect of water and CO₂ in the air was eliminated. The reflected light was collected at
150 the same angle of incidence. The spectra were recorded over the range of 4000-400 cm⁻¹ by using a
151 liquid-nitrogen cooled HgCdTe (MCT) detector. An average of 2000 scans was collected for each
152 spectrum at a resolution of 8 cm⁻¹.

153 **3. Results and discussion**

154 **3.1. Surface pressure–area isotherm**

155 The pressure-induced phase behavior was studied to reveal the underlying phase information of the
156 monolayers being subjected to constant compression. The π -A isotherms for both single and mixed
157 monolayers in different proportions were obtained on the pure water subphase, as illustrated in Figs.
158 1(a)-(c).

159



160

161 **Fig. 1.** Surface pressure (π)–area (A) isotherms of mixed (a) SA/cholesterol, (b) SA/stigmasterol, and
 162 (c) SA/ergosterol monolayers on pure water subphase. (X_{chol} , X_{stig} , and X_{erg} are the molar fractions of
 163 sterols in the mixture)

164

165 It can be seen from Fig. 1(a) that the π – A isotherm of the SA monolayer is in agreement with
 166 that of typical fatty acids (Ma and Allen, 2007), showing four distinct regions based on the changes
 167 in the slope of the isotherm as follows: one at low surface pressures corresponding to an gaseous-
 168 tilted condensed (G-TC) coexistence phase before the lift-off area; a tilted condensed (TC) phase with
 169 less spatial movements for the fatty acid molecules; a third region, where surface pressure increases
 170 abruptly as the monolayer is compressed, consistent with the presence of a untilted condensed (UC)

171 phase; and a collapse phase appearing when the compression isotherm exhibits a sharp spike followed
172 by a drop in surface pressure. This occurrence of SA monolayer collapse has been ascribed to the
173 transformation of a two-dimensional (2D) to a three-dimensional (3D) state upon further compression
174 (Griffith et al., 2012; Kundu and Langevin, 2008; Seoane et al., 2000b). The lift-off area corresponds
175 to the point where the surface organization changes from a G-TC coexistence phase to a TC phase.
176 In the present work, the lift-off area of SA monolayer ($24.76 \text{ \AA}^2/\text{molecule}$) is in good agreement with
177 previous reported values (Sierra-Hernandez and Allen, 2010). The kink appearing in the isotherm at
178 approximately 21.65 mN/m and $16.16 \text{ \AA}^2/\text{molecule}$ indicates the second-order phase transition from
179 the TC to UC state. After phase transition, the conformational order in the hydrocarbon chains
180 increases significantly (Larsen, 2014), with hydrocarbon chains almost perpendicular to the water
181 subphase and packed in a highly ordered structure. The π -A isotherm of the SA monolayer, along
182 with graphical presentation of different phases are given in Fig. S2 for better understanding.

183 It is known from Fig. 1(a) that the π -A isotherm of the cholesterol monolayer shows a rapid rise
184 of surface pressure starting from the lift-off area, despite its bulky hydrocarbon structure and its plate-
185 like steroid ring. Beyond the lift-off point, the slope of the isothermal curve increases steeply and
186 monotonously with the formation of a UC phase before a collapse occurs. The low compressibility
187 and the sharp slope of the isotherm suggests that the cholesterol monolayer is rather rigid and with
188 little reorientation of the sterol molecules during compression. The shape of the π -A isotherm of
189 cholesterol is typical for UC monolayer (Hac-Wydro et al., 2005; Nagadome et al., 2007). As it has
190 already been found (Minones et al., 2009; Seoane et al., 2000a; Seoane et al., 2000b; Sparr et al.,
191 2001) that cholesterol forms a high condensed monolayer, with lift-off area of $38.5 \text{ \AA}^2/\text{molecule}$. Like
192 the one of cholesterol, stigmasterol and ergosterol monolayers on water are also highly condensed,
193 with the lift-off area increasing from $38.5 \text{ \AA}^2/\text{molecule}$ to 42.96 and $44.88 \text{ \AA}^2/\text{molecule}$, respectively
194 (Figs. 1(b) and 1(c)). It follows that the packing order among the respective sterol monolayers
195 decrease in the order cholesterol > stigmasterol > ergosterol.

196 It can be seen from Figs. 1(a)-(c) that all the π -A isotherms of the binary monolayers are
197 localized between those of one component films. The π -A isotherms of all the three SA/sterol mixed
198 monolayers display similar phase behaviors at $X_{\text{chol/stig/erg}} = 0.1$ to that of pure SA but, with less
199 pronounced phase transitions and larger lift-off areas. This indicates that the introduction of a small
200 amount of sterol can influence the main phase transition of SA. The characteristic behavior of SA
201 isotherms disappears even at high SA levels ($X_{\text{SA}} = 0.7$). The isotherms recorded for other mixing

202 ratios ($X_{\text{chol/stig/erg}} = 0.3, 0.5, 0.7$) exhibit no second order phase transition, with surface phase behavior
203 analogous to that of pure sterols. Previous studies about mixed palmitic acid/cholesterol and
204 SA/cholesterol monolayers have also described the gradually disappearance of phase transition of
205 fatty acids on increasing the cholesterol content (Seoane et al., 2000b; Sparr et al., 1999). Thus, the
206 phase behavior of SA/sterol mixed monolayer is governed by the sterols. Attention should be paid to
207 the order of appearance in terms of mole fraction. The high mole fraction of sterols makes the
208 isotherms to have high mean molecular areas and closer to that of each pure sterol. This tendency is
209 consistent with previous observations about mixed cholesterol/fatty acid monolayers (Motomura et
210 al., 1976; Sparr et al., 1999). Consequently, it can be concluded that sterols exert expanding effect on
211 SA monolayer, which suggests the existence of strong interactions between SA and the sterols.

212 Sterol-induced expansion on mixed sterol/SA monolayers can be quantitatively measured by
213 molecular area determinations made on monolayers. The lift-off area of the mixture $X_{\text{chol}} = 0.1$ (25.95
214 $\text{\AA}^2/\text{molecule}$) occupies smaller mean molecular area than those of $X_{\text{stig}} = 0.1$ (26.50 $\text{\AA}^2/\text{molecule}$) and
215 $X_{\text{erg}} = 0.1$ (27.60 $\text{\AA}^2/\text{molecule}$). Similar observations hold for isotherms obtained at other mixing
216 ratios, which indicate that mixed monolayers of SA with cholesterol are more tightly packed than
217 SA/stigmasterol and SA/ergosterol. Higher packing density facilitates more orderly packed alkyl
218 chains thus lead to higher monolayer stability (Tang et al., 2010). Consequently, the order of stability
219 in mixed monolayers can be deduced based on the lift-off areas: cholesterol/SA > SA/stigmasterol >
220 SA/ergosterol, which suggests that stigmasterol and ergosterol are more efficient than chol in
221 disturbing the orderly packed SA monolayer. Cholesterol was shown to condense surface monolayers
222 composed of many, but not all, phospholipids and unsaturated long chain fatty acids (Stillwell et al.,
223 1994; Su et al., 2007). However, we observed that cholesterol exerts an expanding effect on saturated
224 fatty acid monolayers. Similar to cholesterol, stigmasterol and ergosterol also alter SA monolayer
225 properties and induce expanding and disordering effects on fatty acids.

226 The difference between the packing order of sterol monolayers lies in their chemical structure.
227 The bulkier hydrophobic moiety of stigmasterol and ergosterol makes the areas of these two
228 molecules larger than that of cholesterol, thus resulting in more dispersedly packed monolayers. So
229 are the mixtures of stigmasterol and ergosterol with SA compared to the cholesterol/SA films. The
230 bulkier alkyl moiety may cause steric hindrance for highly ordered arrangement of the binary lipid
231 systems. For stigmasterol, the additional ethyl group on the alkyl chain makes it bulkier than
232 cholesterol, preventing it from packing tightly above the water surface, thus decreasing the chain-

233 chain interactions. On the other hand, the additional double bond in stigmasterol may affect the free
234 rotation of the side chain when the molecule comes into contact with SA to form ordered structures
235 (Hac-Wydro et al., 2007). Ergosterol, on the other hand, possesses an additional methyl group and a
236 double bond in the side chain as well as the other one in the sterol ring. Similar with stigmasterol, the
237 presence of an unsaturated bond and methyl group in the hydrocarbon chain makes the molecule more
238 rigid and hinders its conformational freedom (Seoane et al., 1998). It follows that the side
239 hydrocarbon tail, which is stiffer and more elongated than that of cholesterol, protrudes out of the
240 cyclic part of the molecule. As a result, the monolayer of ergosterol is looser than closely packed
241 cholesterol monolayers (Hac-Wydro et al., 2008). In addition, the larger molecular areas occupied by
242 SA/ergosterol compared to that of SA/stigmasterol may origin form the additional double bond
243 present in the cyclic rings of ergosterol, which make its molecular structure stiffer than stigmasterol
244 (Cournia et al., 2007; Gagos and Arczewska, 2012).

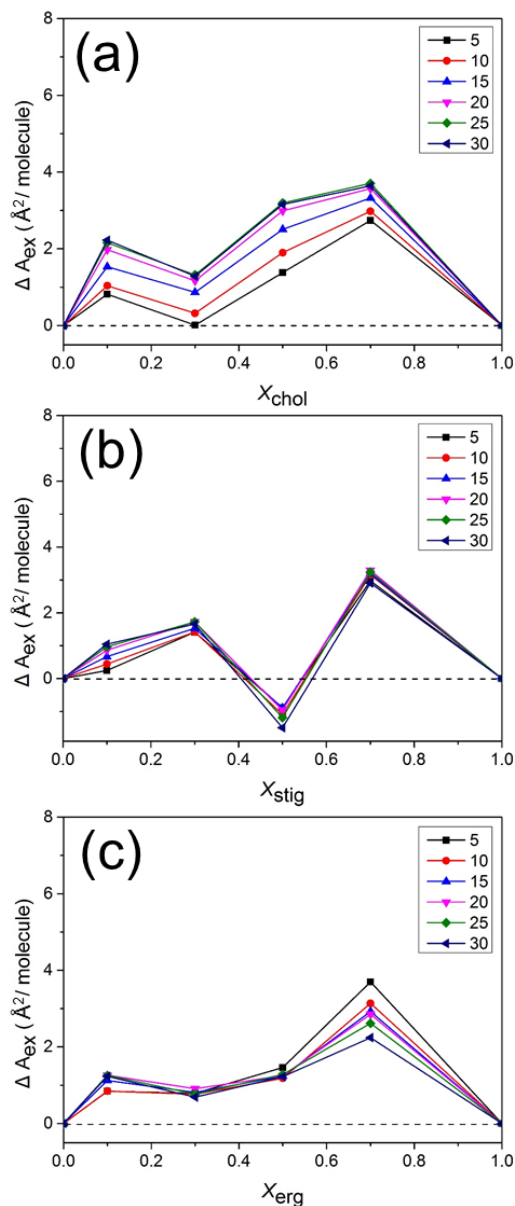
245 Expanding and condensing effects on SA monolayer due to varying X_{sterols} and differences in the
246 molecular structure were assessed from the π -A isotherms. As illustrated in Fig. 1, both the SA/sterol
247 mixing ratios and the functionality of the hydrophobic group affect the molecular packing and thus
248 the degree of molecular interactions between film components. Among the three systems studied, the
249 SA/cholesterol exhibits the strongest stability and SA/ergosterol the weakest, while SA/stigmasterol
250 shows an intermediate behavior. This may result from the interactions between both components that
251 vary with the nature and composition of the system. This consideration led us to examine the
252 miscibility and stability of the two components at the air-water interface.

253 **3.2. Miscibility and stability of the mixed monolayers**

254 Based on the π -A isotherms obtained from Langmuir monolayers for the respective single component
255 and SA/sterol mixed systems, thermodynamic properties have been examined in terms of the excess
256 areas of mixing (ΔA_{ex}) and the excess Gibbs free energy of mixing (ΔG_{ex}). The miscibility between
257 components and the nature of molecular interactions in mixed monolayers can be clarified with the
258 aid of ΔA_{ex} , which is the difference between the real mean molecular area occupied by the mixed
259 monolayer and the area it would occupy if the components of the mixed film behaved in the ideal
260 manner. ΔA_{ex} can be calculated by the following equation (Szczes et al., 2012):

$$261 \quad \Delta A_{\text{ex}} = A_{12} - (A_1X_1 + A_2X_2) \quad (1)$$

262 where A_{12} , A_1 and A_2 represent the real area of the mixed system and the respective areas of pure
263 components 1 and 2 at the same pressure, X_1 and X_2 denote the mole fractions of each component. In
264 fact, ΔA_{ex} quantifies the deviation of the mixture components from the ideality. If the two components
265 are immiscible or ideally miscible, the molecular areas conform to the additivity rule (i.e., the excess
266 area in Equation 1 is zero), while positive or negative deviations from the additivity rule are indicative
267 of miscibility and some degree of molecular interactions between the two components (Seoane et al.,
268 1998). Positive deviations suggest some type of repulsive interactions in the mixed monolayers, while
269 in contrast, negative deviations indicate that attractive interactions exist between the two components
270 (Seoane et al., 1998; Wang et al., 2012). The ΔA_{ex} for the mixed monolayers at constant surface
271 pressures are plotted against the mole fraction of sterols. Figs. 2(a)-(c) show such a dependence for
272 the three SA/sterol systems at different surface pressures including 5, 10, 15, 20, 25 and 30 mN/m.



273

274 **Fig. 2.** Excess molecular areas of mixing (ΔA_{ex}) of the mixed (a) SA/cholesterol, (b) SA/stigmasterol,
 275 and (c) SA/ergosterol monolayers on pure water subphase at the surface pressure of 5, 10, 15, 20, 25
 276 and 30 mN/m. (X_{chol} , X_{stig} , and X_{erg} are the molar fractions of sterols in the mixture)

277

278 As can be seen from Fig. 2, all the ΔA_{ex} of the investigated systems exhibit significant deviations
 279 from ideally mixed film, indicating miscibility of the components in the whole range of surface
 280 pressures and mole ratios. There are always positive deviations for the mole ratios examined, except
 281 for small negative deviations in the equimolar mixture of SA and stigmasterol, suggesting that
 282 repulsive interactions exist between SA and sterols. Consequently, we can speculate that long chain

283 saturated fatty acids and sterols are miscible in the condensed state in a non-ideal behavior, because
284 they are so markedly different in chemical structure (Hac-Wydro and Wydro, 2007; Ouimet et al.,
285 2003).

286 Comparing Figs. 2(a)-(c), a very clear distinction can be found between the interaction of
287 cholesterol, stigmasterol and ergosterol with SA. The data points exhibit positive deviations from the
288 ideal behavior in the mixed SA/cholesterol monolayers, showing that the net repulsive interaction
289 predominates between the components in the SA/cholesterol system, which is in line with a former
290 study (Hac-Wydro and Wydro, 2007). The ΔA_{ex} at all the X_{chol} generally increase with increasing
291 surface pressure, which indicates that the character of the interaction between two components in the
292 SA/cholesterol monolayer shows dependence on the surface pressure. The smallest deviation from
293 ideally mixed film occurs at the surface pressure of 5 mN/m and at the compositions of $X_{\text{chol}} = 0.3$.
294 For the SA/stigmasterol system, no obvious changes in ΔA_{ex} can be observed along with the surface
295 pressures, indicating that the molecules are hardly changed upon compression. The minimum values
296 of ΔA_{ex} for the mixed SA/stigmasterol monolayer are observed at $X_{\text{stig}} = 0.5$ in the whole range of
297 mole fractions, with the lowest negative value obtained at a high surface pressure of 30 mN/m.
298 Regarding SA/ergosterol mixtures, the ΔA_{ex} values are positive, which is a clear indication of
299 expulsive interaction between SA and ergosterol. Like the mixed SA/stigmasterol monolayers, the
300 ΔA_{ex} values at a certain mixing ratio show no obvious changes along with surface pressure, especially
301 at $X_{\text{erg}} = 0.1, 0.3$ and 0.5 . In addition, the general trend of ΔA_{ex} values at a definite surface pressure is
302 becoming more positive with increasing X_{erg} . As displayed in Fig. 2, the largest positive deviation
303 can be observed at $X_{\text{erg}} = 0.7$ for the SA/ergosterol system, which is in line with the other two systems,
304 indicating that the binary mixtures are the most unstable at the ratio of $X_{\text{sterol}} = 0.7$. The positive
305 deviations from zero caused by sterols reveal an increased mean molecular area with respect to the
306 corresponding ideally mixed monolayers, and demonstrate the expanding effect of sterols toward SA
307 monolayer. The deviations from ideal behavior result from the existence of mutual interactions
308 between components present in mixed monolayers (Hac-Wydro et al., 2005).

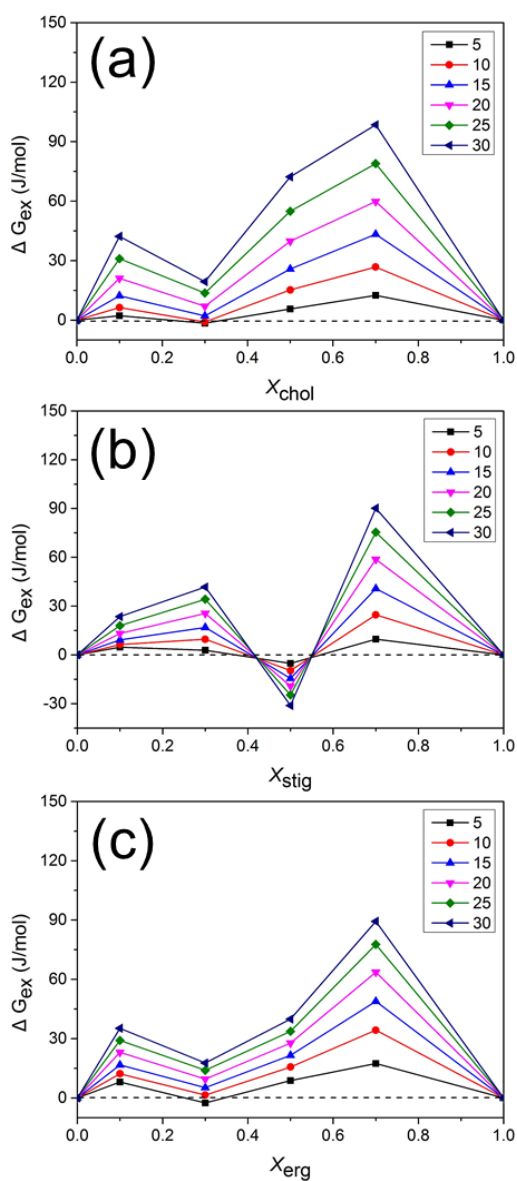
309 From the thermodynamic point of view, the interactions between molecules in the mixed film
310 can be determined quantitatively based on the values of the ΔG_{ex} , which is a measurement of the
311 thermodynamic stability of the mixed monolayer. ΔG_{ex} values can be obtained by integrating the area
312 under the π -A isotherms of pure components and mixed monolayers from zero to a defined pressure,
313 as illustrated by equation 2 (Khattari et al., 2015; Seoane et al., 2000a):

314

$$\Delta G_{\text{ex}} = \int_0^\pi [A_{12} - (X_1 A_1 + X_2 A_2)] d\pi \quad (2)$$

315 From this equation, it can be deduced that if the two components are immiscible or ideally mixed, the
 316 integrand $A_{12} - (A_1 X_1 + A_2 X_2)$ and ΔG_{ex} should be equal to zero at any pressure and mole fraction
 317 (Nagadome et al., 2007; Xie et al., 2005). Mixtures with more negative ΔG_{ex} values are more
 318 thermodynamically stable (Mao et al., 2013). The ΔG_{ex} values were calculated and plotted as a
 319 function of X_{sterols} at selected surface pressures in the range of 0-30 mN/m (Figs. 3(a)-(c)).

320



321

322 **Fig. 3.** Excess Gibbs free energy (ΔG_{ex}) of the mixed (a) SA/cholesterol, (b) SA/stigmasterol, and (c)
323 SA/ergosterol monolayers on pure water subphase at the surface pressure of 5, 10, 15, 20, 25 and 30
324 mN/m. (X_{chol} , X_{stig} , and X_{erg} are the molar fractions of sterols in the mixture)

325

326 The nonzero ΔG_{ex} values presented in Fig. 3 indicate that mixing between SA and sterols is taking
327 place. The general trend of ΔG_{ex} for the three SA/sterol systems is that it becomes more positive as
328 the surface pressure increases, indicating the lower thermostability of more condensed monolayers.
329 From Fig. 3(a), it is worth noting that the values of ΔG_{ex} for SA/cholesterol mixtures are all positive
330 at low and high mole fractions of cholesterol. This suggests that repulsive interactions exist between
331 the monolayers components. It is necessary to relate this to the previous π -A isotherms. Even a very
332 small addition of cholesterol into the SA monolayer significantly expands the latter, thus lowering
333 the strength of interactions with respect to pure SA film. In addition, it can be evidenced from Fig.
334 3(a) that the maximum positive value of ΔG_{ex} for mixed SA/cholesterol films occurs at $X_{\text{chol}} = 0.7$,
335 while the weakest repulsive interactions between SA and sterol molecules correspond to the mixtures
336 at $X_{\text{chol}} = 0.3$. As can be seen from Fig. 3(b), all ΔG_{ex} values are positive at mixing ratios of $X_{\text{stig}} =$
337 0.1, 0.3 and 0.7. This indicates that the mixed SA/stigmasterol monolayers are less stable than they
338 would be if they were formed by components exhibiting an ideal behaviour. The small negative
339 deviations of ΔG_{ex} can be observed at $X_{\text{stig}} = 0.5$, suggesting the formation of most stable mixed
340 monolayers with equimolecular stigmasterol and SA. From the distribution of the ΔG_{ex} values in Fig.
341 3(c), it can be found that ergosterol interacts with SA very similarly to cholesterol in the whole range
342 of compositions and surface pressures studied here. All the mixed SA/ergosterol monolayers are less
343 stable with increasing surface pressure, irrespective of mixing ratios. With respect to the
344 concentration dependence of ΔG_{ex} at a certain pressure, it can be seen that the largest value appears
345 at $X_{\text{erg}} = 0.7$ and the smallest at $X_{\text{erg}} = 0.3$. The positive values of ΔG_{ex} confirm that SA and sterols
346 exhibit miscibility at $T = 294 \pm 1$ K in the whole range of compositions and surface pressures, with
347 the strongest repulsive interaction appearing at $X_{\text{sterol}} = 0.7$.

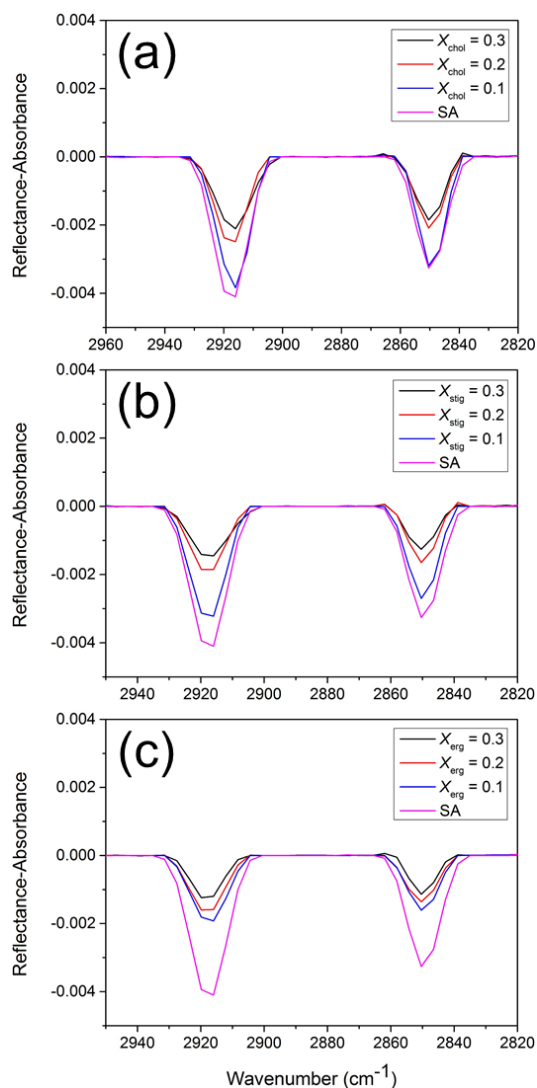
348 The effects of sterols on the phase behavior of SA monolayer were determined here by π -A
349 isotherms recorded on a Langmuir trough. The π -A isotherms provide thermodynamic information
350 about the interaction between sterols and SA from a macroscopic scale. The ΔA_{ex} and ΔG_{ex} derived
351 from the π -A isotherms allowed us to draw conclusions regarding the monolayer components
352 miscibility as well as the kind (repulsive) of interaction between film-forming molecules. The above

353 discussions indicate that, all the three systems are nonideal and miscible. In addition, although
354 cholesterol, stigmasterol and ergosterol have similar chemical structures, their effects on SA
355 monolayer are different, and the specific chemical structures of these molecules are assumed to be
356 the cause of the effects that are observed in the SA/sterol systems. To account for the different
357 interaction mechanisms that have resulted in the discrepancies at the molecular level, PM-IRRAS
358 was chosen as a fast and nondestructive technique to obtain further information of the monolayers.

359 **3.3. PM-IRRAS spectra**

360 PM-IRRAS technique was employed for its surface specificity and molecular level sensitivity.
361 The application of PM-IRRAS allows in-situ characterization of Langmuir films at the air-water
362 interface with regard to the order of the hydrophobic alkyl chains. The IRRAS spectra were obtained
363 at the surface pressure of 26 mN/m, which is representative of SA spectra in the UC phase. IRRAS
364 spectra recorded for SA and mixed SA/sterol monolayers at mixing ratios of $X_{\text{sterol}}=0.1, 0.2$ and 0.3
365 in the C-H stretching region are shown in Figs. 4(a)-(c).

366



367

368 **Fig. 4.** IRRAS spectra of 2950-2820 cm^{-1} region for mixed (a) SA/cholesterol, (b) SA/stigmasterol,
 369 and (c) SA/ergosterol monolayers on pure water subphase recorded at the incidence angle of 40° and
 370 surface pressure of 26 mN/m. (X_{chol} , X_{stig} , and X_{erg} are the molar fractions of sterols in the mixture)

371

372 The investigation of conformational orders of the alkyl chains are mostly based on the methene
 373 (CH_2) stretching vibration bands. At the surface pressure of approximately 26 mN/m, the two strong
 374 and negative bands appearing at about 2916 and 2851 cm^{-1} can be assigned to the asymmetric and
 375 symmetric CH_2 stretching vibrations [$\nu_{\text{a}}(\text{CH}_2)$ and $\nu_{\text{s}}(\text{CH}_2)$] of alkyl chains, respectively (Gericke and
 376 Hühnerfuss, 1993). The frequencies of $\nu_{\text{a}}(\text{CH}_2)$ and $\nu_{\text{s}}(\text{CH}_2)$ stretching vibration are sensitive markers,
 377 which provide a qualitative measure of conformational order and packing in the hydrocarbon chains
 378 (Gericke and Hühnerfuss, 1993; Wang et al., 2012). Lower wavenumbers are characteristic of highly

379 ordered alkyl chains in *all-trans* conformations, while higher wavenumbers denotes disordered chains
380 with *gauche* defects. For *all-trans* conformations of the fully extended tail chains, the symmetric and
381 asymmetric stretching vibrations of the methylene groups are usually present in the narrow ranges of
382 2846-2850 and 2915-2918 cm^{-1} , respectively, and in the distinctly different ranges of 2854-2856 and
383 2924-2928 cm^{-1} for disordered chains characterized by a significant presence of *gauche*
384 conformations (Chen et al., 2012). From the relatively low values of the $\nu_a(\text{CH}_2)$ and $\nu_s(\text{CH}_2)$
385 stretching vibrations studied here, it is clear that the alkyl chains in these monolayers are in mostly
386 high-ordered *all-trans* conformations with few *gauche* defects. Because the surface pressure directly
387 correlates with the van der Waals interaction between adjacent hydrocarbon chains, an orderly packed
388 structure can maximize interactions with *all-trans* conformations (Tang et al., 2010).

389 The f IRRAS peak intensities allow the determination of the orientation of the alkyl chains. Since
390 the directions of both the $\nu_a(\text{CH}_2)$ and $\nu_s(\text{CH}_2)$ modes are orthogonal to the molecular axis, strong
391 intensities of the bands indicate that the molecule stands nearly perpendicular to the water surface
392 when the hydrocarbon chain is in the *all-trans* conformation (Muro et al., 2010). Upon gradual
393 increase of cholesterol levels, obvious decrease in $\nu_a(\text{CH}_2)$ and $\nu_s(\text{CH}_2)$ band intensities is observed
394 (Fig. 4a), which indicates the less ordered alkyl chain in SA monolayer introduced by the existence
395 of sterols. In other words, the interactions between cholesterol and SA decrease the structure order of
396 the SA hydrocarbon chains and, thus, result in an decrease in the packing order of the monolayer.
397 Meanwhile, in the mixed SA/sterol monolayers, sterols provide negligible contribution to the
398 methylene stretching band intensity compared to SA due to its structure with short alkyl chains. A
399 former control experiment conducted on pure cholesterol monolayers did not show any interference
400 in the 2850 cm^{-1} region (Flach et al., 2000). Similarly, a reference PM-IRRAS spectrum of pure
401 ergosterol monolayer deposited at the air-water interface did not show any absorbance (Nasir and
402 Besson, 2012). This feature of sterols is helpful to the interpretation of intensities in relation to the
403 packing order of SA monolayer, as the intensity contribution from sterols can be considered as null
404 or negligible.

405 To investigate the nature of the sterols on the CH_2 stretching bands, Figs. S3(a)-(c) are given to
406 facilitate a direct comparison. It can be seen that at the same sterol levels, the intensities of $\nu_a(\text{CH}_2)$
407 and $\nu_s(\text{CH}_2)$ stretching vibration bands vary with the kind of sterol present in the mixed monolayers,
408 both following the order SA/cholesterol > SA/stigmasterol > SA/ergosterol. This trend agrees well
409 with that predicted from the π -A isotherms, thus, supporting the former conclusion that the stability

410 of the SA/cholesterol system is higher than those of SA/stigmasterol and SA/ergosterol systems, while
411 SA/stigmasterol shows an intermediate behavior. Therefore, the monolayer properties are affected by
412 the presence of the double bond and side chain in the nonpolar residue of the sterol molecules.

413 IRRAS spectra in the C-H stretching region directly reveal the conformational order of the
414 hydrocarbon chains in the monolayers by analyzing the relative intensity of the $\nu_a(\text{CH}_2)$ and the
415 $\nu_s(\text{CH}_2)$ peaks (I_{as}/I_s) (Li et al., 2017). I_{as}/I_s is frequently used as a qualitative indicator to determine
416 the orientation order of the hydrocarbon tails with respect to the surface normal, with a higher value
417 corresponding to alkyl chains with more *trans* bonds (Aoki et al., 2016; Huang et al., 1982; Levin et
418 al., 1985). The peak intensity ratios for mixed SA/sterol monolayers are given in Table S1. As can be
419 seen from the table, the I_{as}/I_s ratios for the mixed SA/sterol monolayers decrease with increasing sterol
420 mole fractions, ranging from 1.21 to 1.14 for SA/cholesterol, 1.19 to 1.13 for SA/stigmasterol and
421 from 1.18 to 1.09 for SA/ergosterol. Meanwhile, all the intensity ratios are lower than that of pure SA
422 monolayer, indicating the disturbing effect of sterols on SA monolayer. In addition, the I_{as}/I_s ratios
423 for mixed SA/cholesterol monolayers are higher than corresponding mixing ratios for mixed
424 SA/stigmasterol monolayers, which in turn are higher than those of mixed SA/ergosterol monolayers.

425 By using PM-IRRAS spectroscopy, evidences of monolayer structure and conformation changes
426 are provided mainly by details of the $\nu_a(\text{CH}_2)$ and $\nu_s(\text{CH}_2)$ stretching vibrations including peak
427 position (wavenumber), peak height and I_{as}/I_s . The above analysis suggests that the mixed SA/sterol
428 monolayers become less condensed in this order: cholesterol/SA > stigmasterol/SA > ergosterol/SA.
429 These changes correlate well with the expected reduction in the packing order of the mixing
430 monolayers due to the nature of sterols as was shown by the surface pressure–area isotherms.

431 **3.4. Atmospheric implications**

432 The presence of surface-active organic compounds at the SML has been found to be ubiquitous
433 (Cochran et al., 2016a; Cochran et al., 2016b). A significant quantity of surfactant materials
434 transported to the atmosphere from the ocean is mediated by bursting bubbles, which scavenge
435 surface-active organic compounds and other materials from the seawater (Bertram et al., 2018;
436 Tervahattu et al., 2002; Tseng et al., 1992). These surface-active organic compounds ultimately form
437 thin films that affect physical and chemical properties of marine aerosols (Gilman et al., 2006;
438 Rouviere and Ammann, 2010; Vaida, 2016). Thus, investigation of the surface properties of model
439 organic films will improve our understanding about the environmental impacts of SSAs. Surface-

440 active species present at the interface of marine aerosols are dominated by fatty acids with
441 hydrocarbon chain lengths of C16 and C18 (Ellison et al., 1999; Rouviere and Ammann, 2010). As
442 an important class of surfactants present at the SML and interface of SSAs (Bertram et al., 2018), the
443 effect of sterols on surface properties of SSA has not received much attention and yet to be fully
444 elucidated. Systems consisting of SA and sterols of different structures (cholesterol, ergosterol and
445 stigmasterol) spread at the air-water interface were used to form mixed monolayers, the components
446 of which were found to interact with each other. The increase in lift-off area of SA monolayer
447 indicates the expanding effect of sterols and further lowering effect on its stability. In addition, it was
448 shown that the nature of the sterols plays a role in the interaction of SA, with SA/cholesterol
449 exhibiting the strongest stability, followed by SA/stigmasterol, while SA/ergosterol exhibits the
450 weakest stability.

451 Investigation of molecular interactions enables examination of surface processes such as the mass
452 transport of water and trace gases through the interface of aerosols (Bertram et al., 2018; Cosman and
453 Bertram, 2008). The film condensation and expansion processes have the potential to further
454 influence the particle's size through altering its ability to evaporate or absorb water and radiative
455 properties (Davies et al., 2013; Vaida, 2016), as the scattering efficiency of aerosol particles has a
456 strong dependency on their size (Adams and Allen, 2013). The measurements here support the notion
457 that SA/stigmasterol and SA/ergosterol are more loosely packed, and thus more likely to induce the
458 penetration of water into the lipid monolayers. Moreover, the uptake of chemical species such as
459 N_2O_5 and HNO_3 into atmospheric aerosol particles will further facilitates chemical reactions inside
460 the aqueous core (McNeill et al., 2006; Thornton and Abbatt, 2005). The surface-active organic
461 monolayer has been shown to play an important role in the lowering of the permeability of trace gases
462 and other volatile species to transport through the aerosols interface (Bertram et al., 2018; Cosman
463 and Bertram, 2008; Davies et al., 2013). For ambient aerosols, it can be largely assumed that the high
464 complexity of organic composition prevents the formation of condensed film required for suppression
465 of trace gases transport (Davies et al., 2013) With higher packing order and stability, it is shown here
466 that SA monolayer will be more effective at "blocking" interfacial transport than mixed SA/sterol
467 monolayers. Consequently, the incorporation of sterols will lead to the presence of defects on the
468 organic films of marine aerosols due to complex component interactions, thus limit the importance of
469 this potential process.

470 Therefore, the surface properties of the SA monolayer altered in the presence of sterols, and that
471 these alterations would result in transformations to the size, reactivity, and ability of aerosol particles
472 to scatter light. The present study is likely to shed light on many boundary processes taking place at
473 the interface of SSAs, and transport processes of water and trace gases across the interface, in
474 particular.

475 **4. Conclusions**

476 In this work, mixed SA/sterol monolayer systems were chosen as proxies to determine how the
477 concentration and nature of sterols impact the surface properties of marine aerosols, and to understand
478 the underlying mechanisms. Properties of the monolayers were analyzed based on the parameters
479 derived from the π -A isotherms and PM-IRRAS spectra. From the π -A isotherms obtained from
480 Langmuir experiments, it was found that SA forms high orderly packed monolayer at the air-water
481 interface, which undergoes expansion upon addition of sterols. Ergosterol induces a much more
482 pronounced expanding effect on lift-off area of SA than cholesterol, while stigmasterol shows an
483 intermediate behavior, leading to the following order: SA/cholesterol > SA/stigmasterol >
484 SA/ergosterol. The interactions inside binary mixture monolayers have been analyzed in terms of
485 thermodynamic parameters including excess molecular area and excess Gibbs free energy of mixing,
486 which revealed that repulsive forces between SA and sterol molecules are the main driving force for
487 the expanding effect seen at the monolayer systems. The decrease in conformational order of SA
488 monolayer upon addition of sterols can also be evidenced by the lower peak intensities of $\nu_a(\text{CH}_2)$
489 and $\nu_s(\text{CH}_2)$. The observed difference in the interactions of the sterols with SA is related to the specific
490 structures of the sterol molecules. The bulkier hydrophobic portion of stigmasterol and ergosterol
491 arising from the additional alkyl groups and double bonds, which manifest as reduced packing
492 effectiveness, increased tilt of the molecules with respect to the monolayer plane, and augmented
493 penetration of water into marine aerosols.

494

495 **Acknowledgements**

496 This work was supported by National Natural Science Foundation of China (91644214, 21876098),
497 Shandong Natural Science Fund for Distinguished Young Scholars (JQ201705) and Marie Curie
498 International Research Staff Exchange project MARSU (Grant 690958).

499

500 **Conflicts of interest**

501 The authors declare no conflicts of interest.

502

503 **Supplementary data**

504 Chemical structures of the sterols used in this study (Fig. S1), the π -A isotherm of the SA monolayer
505 along with graphical presentation of different monolayers phases (Fig. S2), IRRAS spectra of 2950-
506 2820 cm^{-1} region for the mixed SA/sterol monolayers on pure water subphase recorded at the
507 incidence angle of 40° and surface pressure of 26 mN/m (Fig. S3), and the peak-height intensity ratio
508 between the asymmetric and symmetric bands of the CH_2 groups ($I_{\text{as}}/I_{\text{s}}$) for the mixed SA/sterol
509 monolayers on pure water subphase (Table S1).

510

511 **Reference**

- 512 Adams E.M., Allen H.C., 2013. Palmitic acid on salt subphases and in mixed monolayers of
513 cerebrosides: Application to atmospheric aerosol chemistry. *Atmosphere* 4, 315-336.
- 514 Adams E.M., Casper C.B., Allen H.C., 2016. Effect of cation enrichment on
515 dipalmitoylphosphatidylcholine (DPPC) monolayers at the air-water interface. *J. Colloid*
516 *Interface Sci.* 478, 353-364.
- 517 Aoki P.H.B., Morato L.F.C., Pavinatto F.J., Nobre T.M., Constantino C.J.L., Oliveira O.N., Jr., 2016.
518 Molecular-level modifications induced by photo-oxidation of lipid monolayers interacting
519 with erythrosin. *Langmuir* 32, 3766-3773.
- 520 Barbier M., Tusseau D., Marty J.C., Saliot A., 1981. Sterols in aerosols, surface microlayer and
521 subsurface water in the Northeastern tropical Atlantic. *Oceanol. Acta* 4, 77-84.
- 522 Bertram T.H., Cochran R.E., Grassian V.H., Stone E.A., 2018. Sea spray aerosol chemical
523 composition: elemental and molecular mimics for laboratory studies of heterogeneous and
524 multiphase reactions. *Chem. Soc. Rev.* 47, 2374-2400.
- 525 Chen Q.B., Kang X.L., Li R., Du X.Z., Shang Y.Z., Liu H.L., et al., 2012. Structure of the complex
526 monolayer of Gemini surfactant and DNA at the air/water interface. *Langmuir* 28, 3429-3438.
- 527 Cochran R.E., Jayarathne T., Stone E.A., Grassian V.H., 2016a. Selectivity across the interface: A
528 test of surface activity in the composition of organic-enriched aerosols from bubble bursting.
529 *J. Phys. Chem. Lett.* 7, 1692-1696.
- 530 Cochran R.E., Laskina O., Jayarathne T., Laskin A., Laskin J., Lin P., et al., 2016b. Analysis of
531 organic anionic surfactants in fine and coarse fractions of freshly emitted sea spray aerosol.
532 *Environ. Sci. Technol.* 50, 2477-2486.
- 533 Cosman L.M., Bertram A.K., 2008. Reactive uptake of N_2O_5 on aqueous H_2SO_4 solutions coated with
534 1-component and 2-component monolayers. *J. Phys. Chem. A* 112, 4625-4635.
- 535 Cournia Z., Ullmann G.M., Smith J.C., 2007. Differential effects of cholesterol, ergosterol and
536 lanosterol on a dipalmitoyl phosphatidylcholine membrane: A molecular dynamics simulation
537 study. *J. Phys. Chem. B* 111, 1786-1801.
- 538 Davies J.F., Miles R.E.H., Haddrell A.E., Reid J.P., 2013. Influence of organic films on the
539 evaporation and condensation of water in aerosol. *Proc. Natl. Acad. Sci. U. S. A.* 110, 8807-
540 8812.

- 541 Du X.Z., Wang Y.C., 2007. Directed assembly of binary monolayers with a high protein affinity:
542 Infrared reflection absorption spectroscopy (IRRAS) and surface plasmon resonance (SPR).
543 J. Phys. Chem. B 111, 2347-2356.
- 544 Ellison G.B., Tuck A.F., Vaida V., 1999. Atmospheric processing of organic aerosols. J. Geophys.
545 Res.: Atmos. 104, 11633-11641.
- 546 Flach C.R., Mendelsohn R., Rerek M.E., Moore D.J., 2000. Biophysical studies of model stratum
547 corneum lipid monolayers by Infrared Reflection–Absorption Spectroscopy and Brewster
548 Angle Microscopy. J. Phys. Chem. B 104, 2159-2165.
- 549 Gagos M., Arczewska M., 2012. FTIR spectroscopic study of molecular organization of the antibiotic
550 amphotericin B in aqueous solution and in DPPC lipid monolayers containing the sterols
551 cholesterol and ergosterol. Eur. Biophys. J. Biophys. Lett. 41, 663-673.
- 552 Garland R.M., Wise M.E., Beaver M.R., DeWitt H.L., Aiken A.C., Jimenez J.L., et al., 2005. Impact
553 of palmitic acid coating on the water uptake and loss of ammonium sulfate particles. Atmos.
554 Chem. Phys. 5, 1951-1961.
- 555 Gasparovic B., Frka S., Kozarac Z., Nelson A., 2008. A method for characterization of sea surface
556 microlayer based on monolayer properties in presence and absence of phospholipids. Anal.
557 Chim. Acta 620, 64-72.
- 558 Gašparović B., Kozarac Z., Saliot A., Čosović B., Möbius D., 1998. Physicochemical characterization
559 of natural and ex-situ reconstructed sea-surface microlayers. J. Colloid Interface Sci. 208,
560 191-202.
- 561 Gericke A., Hühnerfuss H., 1993. In-situ investigation of saturated long-chain fatty-acids at the air-
562 water-interface by external infrared reflection-absorption spectrometry. J. Phys. Chem. 97,
563 12899-12908.
- 564 Gilman J.B., Tervahattu H., Vaida V., 2006. Interfacial properties of mixed films of long-chain
565 organics at the air-water interface. Atmos. Environ. 40, 6606-6614.
- 566 Goto T.E., Caseli L., 2013. Understanding the collapse mechanism in Langmuir monolayers through
567 polarization modulation-infrared reflection absorption spectroscopy. Langmuir 29, 9063-
568 9071.
- 569 Griffith E.C., Adams E.M., Allen H.C., Vaida V., 2012. Hydrophobic collapse of a stearic acid film
570 by adsorbed l-phenylalanine at the air-water interface. J. Phys. Chem. B 116, 7849-7857.
- 571 Griffith E.C., Guizado T.R.C., Pimentel A.S., Tyndall G.S., Vaida V., 2013. Oxidized aromatic-
572 aliphatic mixed films at the air-aqueous solution interface. J. Phys. Chem. C 117, 22341-
573 22350.
- 574 Hac-Wydro K., Dynarowicz-Latka P., Grzybowska J., Borowski E., 2008. Interactions between
575 amphotericin B 3-(N',N'-dimethylamino) propyl amide and cellular membrane components
576 in Langmuir monolayers. Thin Solid Films 516, 1197-1203.
- 577 Hac-Wydro K., Wydro P., 2007. The influence of fatty acids on model cholesterol/phospholipid
578 membranes. Chem. Phys. Lipids 150, 66-81.
- 579 Hac-Wydro K., Wydro P., Dynarowicz-Latka P., 2005. Interactions between
580 dialkyldimethylammonium bromides (DXDAB) and sterols - a monolayer study. J. Colloid
581 Interface Sci. 286, 504-510.
- 582 Hac-Wydro K., Wydro P., Jagoda A., Kapusta J., 2007. The study on the interaction between
583 phytosterols and phospholipids in model membranes. Chem. Phys. Lipids 150, 22-34.
- 584 Huang C.H., Lapidus J.R., Levin I.W., 1982. Phase-transition behavior of saturated, symmetric chain
585 phospholipid-bilayer dispersions determined by Raman-spectroscopy-correlation between
586 spectral and thermodynamic parameters. J. Am. Chem. Soc. 104, 5926-5930.

587 Khattari Z., Al-Abdullah T., Maghrabi M., Khasim S., Roy A., Fasfous I., 2015. Interaction study of
588 lipopeptide biosurfactant viscosin with DPPC and cholesterol by Langmuir monolayer
589 technique. *Soft Mater.* 13, 254-262.

590 Khattari Z., Sayyed M.I., Qashou S.I., Fasfous I., Al-Abdullah T., Maghrabi M., 2017. Interfacial
591 behavior of myristic acid in mixtures with DMPC and cholesterol. *Chem. Phys.* 490, 106-114.

592 Kundu S., Langevin D., 2008. Fatty acid monolayer dissociation and collapse: Effect of pH and
593 cations. *Colloid Surf. A-Physicochem. Eng. Asp.* 325, 81-85.

594 Larsen M.C., 2014. Binary phase diagrams at the air-water interface: An experiment for
595 undergraduate physical chemistry students. *J. Chem. Educ.* 91, 597-601.

596 Levin I.W., Thompson T.E., Barenholz Y., Huang C., 1985. Two types of hydrocarbon chain
597 interdigitation in sphingomyelin bilayers. *Biochemistry* 24, 6282-6286.

598 Li S.Y., Du L., Wei Z.M., Wang W.X., 2017. Aqueous-phase aerosols on the air-water interface:
599 Response of fatty acid Langmuir monolayers to atmospheric inorganic ions. *Sci. Total*
600 *Environ.* 580, 1155-1161.

601 Ma G., Allen H.C., 2007. Condensing effect of palmitic acid on DPPC in mixed Langmuir
602 monolayers. *Langmuir* 23, 589-597.

603 Mao G.R., VanWyck D., Xiao X., Correa M.C.M., Gunn E., Flach C.R., et al., 2013. Oleic acid
604 disorders stratum corneum lipids in Langmuir monolayers. *Langmuir* 29, 4857-4865.

605 McNeill V.F., Patterson J., Wolfe G.M., Thornton J.A., 2006. The effect of varying levels of
606 surfactant on the reactive uptake of N₂O₅ to aqueous aerosol. *Atmos. Chem. Phys.* 6, 1635-
607 1644.

608 Minones J., Pais S., Minones J., Conde O., Dynarowicz-Latka P., 2009. Interactions between
609 membrane sterols and phospholipids in model mammalian and fungi cellular membranes - A
610 Langmuir monolayer study. *Biophys. Chem.* 140, 69-77.

611 Motomura K., Terazono T., Matuo H., Matuura R., 1976. Mixed monolayers of cholesterol with fatty
612 acids. *J. Colloid Interface Sci.* 57, 52-57.

613 Muro M., Itoh Y., Hasegawa T., 2010. A conformation and orientation model of the carboxylic group
614 of fatty acids dependent on chain length in a Langmuir monolayer film studied by
615 polarization-modulation infrared reflection absorption spectroscopy. *J. Phys. Chem. B* 114,
616 11496-11501.

617 Nagadome S., Suzuki N.S., Mine Y., Yamaguchi T., Nakahara H., Shibata O., et al., 2007.
618 Monolayers (Langmuir films) behavior of multi-component systems composed of a bile acid
619 with different sterols and with their 1 : 1 mixtures. *Colloid Surf. B-Biointerfaces* 58, 121-136.

620 Nasir M.N., Besson F., 2012. Interactions of the antifungal mycosubtilin with ergosterol-containing
621 interfacial monolayers. *Biochim. Biophys. Acta-Biomembr.* 1818, 1302-1308.

622 Noziere B., Baduel C., Jaffrezo J.L., 2014. The dynamic surface tension of atmospheric aerosol
623 surfactants reveals new aspects of cloud activation. *Nat. Commun.* 5, 3335.

624 Ouimet J., Croft S., Pare C., Katsaras J., Lafleur M., 2003. Modulation of the polymorphism of the
625 palmitic acid/cholesterol system by the pH. *Langmuir* 19, 1089-1097.

626 Prather K.A., Bertram T.H., Grassian V.H., Deane G.B., Stokes M.D., DeMott P.J., et al., 2013.
627 Bringing the ocean into the laboratory to probe the chemical complexity of sea spray aerosol.
628 *Proc. Natl. Acad. Sci. U. S. A.* 110, 7550-7555.

629 Rouviere A., Ammann M., 2010. The effect of fatty acid surfactants on the uptake of ozone to aqueous
630 halogenide particles. *Atmos. Chem. Phys.* 10, 11489-11500.

631 Saliot A., Barbier M., 1973. Sterols from sea-water. *Deep-Sea Res.* 20, 1077-1082.

632 Seoane R., Minones J., Conde O., Casas M., Iribarnegaray E., 1998. Molecular organisation of
633 amphotericin B at the air-water interface in the presence of sterols: a monolayer study.
634 *Biochim. Biophys. Acta-Biomembr.* 1375, 73-83.

635 Seoane R., Minones J., Conde O., Minones J., 2000a. Study of the interaction of cholesterol with
636 potentially hypocholesterolemic substances in a monolayer form. *Colloid Surf. A-*
637 *Physicochem. Eng. Asp.* 174, 329-340.

638 Seoane R., Minones J., Conde O., Minones J., Casas M., Iribarnegaray E., 2000b. Thermodynamic
639 and Brewster angle microscopy studies of fatty acid/cholesterol mixtures at the air/water
640 interface. *J. Phys. Chem. B* 104, 7735-7744.

641 Serfis A.B., Brancato S., Fliesler S.J., 2001. Comparative behavior of sterols in phosphatidylcholine-
642 sterol monolayer films. *Biochim. Biophys. Acta-Biomembr.* 1511, 341-348.

643 Shrestha M., Luo M., Li Y.M., Xiang B., Xiong W., Grassian V.H., 2018. Let there be light: stability
644 of palmitic acid monolayers at the air/salt water interface in the presence and absence of
645 simulated solar light and a photosensitizer. *Chem. Sci.* 9, 5716-5723.

646 Sierra-Hernandez M.R., Allen H.C., 2010. Incorporation and exclusion of long chain alkyl halides in
647 fatty acid monolayers at the air-water interface. *Langmuir* 26, 18806-18816.

648 Sparr E., Ekelund K., Engblom J., Engstrom S., Wennerstrom H., 1999. An AFM study of lipid
649 monolayers. 2. Effect of cholesterol on fatty acids. *Langmuir* 15, 6950-6955.

650 Sparr E., Eriksson L., Bouwstra J.A., Ekelund K., 2001. AFM study of lipid monolayers: III. Phase
651 behavior of ceramides, cholesterol and fatty acids. *Langmuir* 17, 164-172.

652 Stillwell W., Ehringer W.D., Dumauil A.C., Wassall S.R., 1994. Cholesterol condensation of α -
653 linolenic and γ -linolenic acid-containing phosphatidylcholine monolayers and bilayers.
654 *Biochim. Biophys. Acta, Lipids Lipid Metab.* 1214, 131-136.

655 Su Y.L., Li Q.Z., Chen L., Yu Z.W., 2007. Condensation effect of cholesterol, stigmaterol, and
656 sitosterol on dipalmitoylphosphatidylcholine in molecular monolayers. *Colloid Surf. A-*
657 *Physicochem. Eng. Asp.* 293, 123-129.

658 Szczes A., Jurak M., Chibowski E., 2012. Stability of binary model membranes-Prediction of the
659 liposome stability by the Langmuir monolayer study. *J. Colloid Interface Sci.* 372, 212-216.

660 Tang C.Y., Huang Z.S.A., Allen H.C., 2010. Binding of Mg^{2+} and Ca^{2+} to palmitic acid and
661 deprotonation of the COOH headgroup studied by vibrational sum frequency generation
662 spectroscopy. *J. Phys. Chem. B* 114, 17068-17076.

663 Tervahattu H., Hartonen K., Kerminen V.M., Kupiainen K., Aamio P., Koskentalo T., et al., 2002.
664 New evidence of an organic layer on marine aerosols. *J. Geophys. Res.* 107, AAC1-AAC9.

665 Thornton J.A., Abbatt J.P.D., 2005. N_2O_5 reaction on submicron sea salt aerosol: Kinetics, products,
666 and the effect of surface active organics. *J. Phys. Chem. A* 109, 10004-10012.

667 Tinel L., Rossignol S., Bianco A., Passananti M., Perrier S., Wang X.M., et al., 2016. Mechanistic
668 insights on the photosensitized chemistry of a fatty acid at the Air/Water interface. *Environ.*
669 *Sci. Technol.* 50, 11041-11048.

670 Tseng R.S., Viechnicki J.T., Skop R.A., Brown J.W., 1992. Sea-to-air transfer of surface-active
671 organic-compounds by bursting bubbles. *J. Geophys. Res.: Oceans* 97, 5201-5206.

672 Vaida V., 2016. Atmospheric radical chemistry revisited Sunlight may directly drive previously
673 unknown organic reactions at environmental surfaces. *Science* 353, 650-650.

674 Wang X.Y., Huang X., Xin Y.Y., Du X.Z., 2012. Myoglobin-directed assemblies of binary
675 monolayers functionalized with iminodiacetic acid ligands at the air-water interface through
676 metal coordination for multivalent protein binding. *Phys. Chem. Chem. Phys.* 14, 5470-5478.

677 Xie A.J., Shen Y.H., Xia B., Chen H.B., Ouyang J.M., 2005. Thermodynamic studies of
678 bilirubin/cholesterol mixtures at the air/water interface. *Thin Solid Films* 472, 227-231.

679 Zhang T., Cathcart M.G., Vidalis A.S., Allen H.C., 2016. Cation effects on phosphatidic acid
680 monolayers at various pH conditions. *Chem. Phys. Lipids* 200, 24-31.

681